Science of the Total Environment 807 (2022) 150481

Contents lists available at ScienceDirect

Science of the Total Environment

journal homepage: www.elsevier.com/locate/scitotenv

Geographical drivers of geochemical and mineralogical evolution of Motianling peatland (Northeast China) exposed to different sources of rare earth elements and Pb, Nd, and Sr isotopes

Barbara Fiałkiewicz-Kozieł [a,*], Kunshan Bao [b], Beata Smieja-Król [c]

[a] Adam Mickiewicz University, Institute of Geoinformation and Geoecology, Krygowskiego 10, Poznań, Poland
[b] School of Geography, South China Normal University, Guangzhou 510631, China
[c] University of Silesia, Institute of Earth Sciences, Faculty of Natural Sciences, Będzińska 60, 41-200 Sosnowiec, Poland

HIGHLIGHTS

- Volcanic bedrock-peat interaction is a main driver of enhanced trophy.
- Northern Chinese deserts and Gobi are main REE providers of natural origin.
- Industrial impact is signed by a decrease in $^{206}Pb/^{207}Pb$, ↑εNd and Gd enrichment.
- Anthropogenic particles have been detected since 1960s.

GRAPHICAL ABSTRACT

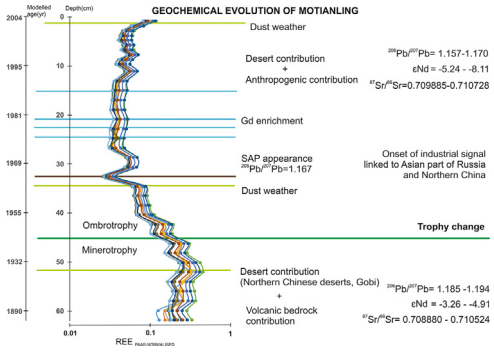

ARTICLE INFO

Article history:
Received 29 June 2021
Received in revised form 15 September 2021
Accepted 16 September 2021
Available online 5 October 2021

Editor: Filip M.G. Tack

Keywords:
Peat bog
Stable isotopes
Rare earth elements
Anthropocene
Source provenance

ABSTRACT

Geochemical shifts triggered by surface runoff and atmospheric fallout in a Chinese peatland were investigated by using Pb, Sr, and Nd, REE and by SEM mineralogical analysis. Motianling peatland (Northeast China) is located at 1670 m a.s.l., near the China–Mongolia border. Based on division of profile into two phases of different trophy, the total ∑REE value determined for the minerotrophic part of the profile (from 62 to 46 cm) varied from 67 to 31 mg·kg^{-1} and mineralogical analysis revealed the occurrence of weathered volcanic rocks, supported by a high εNd value (−3.26). After the transition from minerotrophic to more ombrotrophic conditions, the peatland became independent of the local bedrock weathering, which was manifested by a much lower concentration of REE (7–20 mg·kg^{-1}) and lower εNd values (−7.37; −8.11). Moreover, PAAS-normalized pattern of REE distribution in the bottom part revealed the highest Eu/Eu* value (1.24), as well as a slight enrichment in Eu. The anthropogenic effect was visible from 1964, during which period the spheroidal aluminosilicate particles (SAP), produced by coal-fired power-plant activity, appeared for the first time, followed by an abrupt decrease in $^{206}Pb/^{207}Pb$ isotopic signature to 1.167. The dimensions of SAP (~1.5 μm), as well as the time of first appearance, indicated long-range transport. The REE ratios obtained in this study are characteristic of the eolian deposition signature, which is like the Gobi and northern Chinese deserts. The anthropogenic activity was manifested by a slight enrichment in Gd during reduced delivery of natural dust. Both, North Chinese and Asian part of the Russian industry supply anthropogenic dust. Topography, wind direction, and patterns of precipitation, as well as the initial phases of Asian industrial development, are the most important drivers promoting the deposition of chemical elements.

* Corresponding author.
E-mail address: basiafk@amu.edu.pl (B. Fiałkiewicz-Kozieł).

https://doi.org/10.1016/j.scitotenv.2021.150481

1. Introduction

Arid areas in Central Asia are important sources of dust throughout the world. They contribute to the regional and local soils of China (Sun et al., 2001) and other Asian countries (Miyazaki et al., 2016). The signature of the arid areas has also been evidenced in Greenland (Biscaye et al., 1997; Bory et al., 2003, 2014), North America (McKendry et al., 2007; Sassen, 2002; DeBell et al., 2004; Zdanowicz et al., 2006), and Europe (Grousset et al., 2003). Asia adds dust from industrial sources, e.g., fossil fuels combustion and ore exploitation and processing, with distinguishable centers in Russia (Purvis et al., 2004; Nikitina and Kotov, 1999) and China (Kurokawa et al., 2013; Van Der et al., 2017; Wan et al., 2020). The Chinese anthropogenic signature was detected in Japan (Mukai et al., 1994) and the North Pacific (Gallon et al., 2011), while the Russian one in Nordic countries (Nikitina and Kotov, 1999). Complex wind circulation is critical in assessing the source of aerosols in central Asia (Wang et al., 2011; Wang et al., 2015; Herzschuh et al., 2019). Still, the highest amount of dust is carried by westerlies or winter monsoon, characterized by higher wind speed compared to summer monsoon, whose influence on dust deposition seems insignificant (Lee and Sohn, 2009; Lee and Kim, 2012; Zhang et al., 2021). Moreover, the distance from dust sources to areas of deposition, which decreased exponentially, are an important factor affecting the final signature of dust (Nakano et al., 2004).

The anthropogenic and natural, local, and distant dust emitters can be evaluated by a broad set of methods, from conventional like macroelement analysis and corresponding enrichment factors (Shotyk et al., 2002; Kylander et al., 2006) to more sophisticated like isotopic systems. Lead, Sr, and Nd radiogenic isotopes are considered as powerful tools to reconstruct the provenance of long-range transported dust deposited in environmental archives (e.g., Grousset and Biscaye, 2005; Kamenov et al., 2009; Cheng and Hu, 2010; Le Roux et al., 2012; Fagel et al., 2014). The immobility and utility of these systems are well established. Among the radiogenic isotopes, lead isotopes are widely utilized to distinguish natural (Shotyk et al., 1998a, 1998b; Bollhöfer and Rosman, 2001; Schleicher et al., 2020) and anthropogenic sources of dust (Mukai et al., 1993, 1994, 2001; Erel et al., 1997; Shotyk et al., 1997; Shotyk et al., 1998a, 1998b; Kylander et al., 2006; Geagea et al., 2007, 2008; De Vleeschouwer et al., 2009; Fiałkiewicz-Kozieł et al., 2018; Fiałkiewicz-Kozieł et al., 2020). ^{87}Sr and ^{86}Sr as well $^{143}Nd/^{144}Nd$ are mainly used to track natural processes like the arid areas dust emission and deposition (Biscaye et al., 1997; Nakano et al., 2004, 2005; Grousset and Biscaye, 2005; Sapkota, 2006). Nd isotope studies have reported Sahara as the dominant source of natural dust for Western Europe (Le Roux et al., 2012; Fagel et al., 2014). Recently, an increasing role of Sr and Nd isotopes in determining anthropogenic impact is observed. Kamenov et al. (2009) determined $^{87}Sr/^{86}Sr$ and $^{143}Nd/^{144}Nd$ to assess the impact of anthropogenic activity in salt marsh and observed that the radiogenity of the system decreased due to some anthropogenic activities. Geagea et al. (2007, 2008) established Sr and Nd isotopic signatures of atmospheric aerosols of anthropogenic origin in France. Li et al. (2009) used Nd and Sr to establish the natural and anthropogenic sources of East Asian dust. Similarly, in their study on a Siberian peatland, Fiałkiewicz-Kozieł et al. (2016) noted that after 1950 the radiogenity of Nd and Sr isotopes decreased probably due to human activity.

Rare earth elements (REE) are conservative lithogenic elements used to track the provenance of natural sources (e.g., Kylander et al., 2007; Shotyk et al., 2002; Ferrat et al., 2012b; Le Roux et al., 2012; Fagel et al., 2014; Vanneste et al., 2016; Pratte et al., 2017; Pratte et al., 2020). Recent studies showed the influence of industrial activity linked with coal combustion on REE enrichment in an environmental record, pointing out the utility of REE to trace anthropogenic sources, but only in areas located in the vicinity of industrial centers (Fiałkiewicz-Kozieł et al., 2020).

Peatlands are crucial archives of past environmental changes (Shotyk, 1988; Bindler, 2006) and have been broadly used to assess local, regional and global patterns of naturally or anthropogenically induced dust deposition (Kylander et al., 2006). Many studies were carried out for tracing dust sources and transport patterns in China (Biscaye et al., 1997; Sun et al., 2001; Grousset and Biscaye, 2005; Chen et al., 2007), but only a few focused on peatlands (Bao et al., 2012; Ferrat et al., 2012a, 2012b; Bao et al., 2019; Cong et al., 2019; Pratte et al., 2020).

The Motianling peatland is in the most northern part of China that belongs to a moderate, cold climate with the domination of westerlies. The pattern of elements deposition is expected to be different comparing with eastern or southern regions of China. Many orographic barriers (e.g., Tian Shan and Altai range) effectively block the long-range transport from Kazakhstan or the western part of Russia to the peatland. On the other hand, industrial centers located near the China–Mongolia-Russia border may contribute to deposition of substantial amounts of trace elements.

Herein this study, we analyzed Motianling, a mountain peatland located in Aershan in Great Hinggan Mountains, Northeast (NE) China. This peatland has a well-established trophy status and was previously studied to assess the levels of Pb and Hg pollution and dust deposition (Bao et al., 2010, 2015; Pratte et al., 2018). The influence of dust episodes on Motianling was reported earlier, using macroelements concentration (Bao et al., 2012). While Al, Ca, Fe, Mn, V and Ti are good indicators of enhanced dust delivery, we broadened the set of analytical methods and used REE, Sr, Nd, and Pb isotopes, and performed a detailed mineralogical analysis to understand the geochemical development of the peatland and to distinguish the sources of dust in mountain areas of NE China. We hypothesized that Motianling, as a mountain peatland, nowadays fed mainly by atmospheric sources, located on northern slope of mountain, what successfully isolates from the major southern and eastern Chinese industrial centers, serves as an exceptional model to investigate long-range transport and assess global aerosol input before the great Chinese economic boost.

This study aimed to trace the geochemical evolution of peat, characterized by a significant shift from minerotrophic conditions to more ombrotrophic ones. We assessed the patterns of distribution of REE elements and the Nd and Sr isotopic composition of the peat and distinguished the possible sources of deposited dust by using the REE, mineralogical, and isotopic signatures.

2. Study site and methods

2.1. Study site

Motianling (also known as Gaoshan) is the highest peak (1712 m a.s.l.) in the volcanic Aershan Mountains (46°39′–47°39′ N, 119°28′–121°23′ E). It is located on the western side of the middle section of the Great Hinggan Mountains, near the boundary between China and Mongolia (Fig. 1). The peak formed during the Holocene period and belongs to Stromboli eruption type. The last eruption was in 1990 ± 100 BP. The local geology is dominated by Holocene and Pleistocene alkali-olivine basaltic and scoria cover over Jurassic volcanic-plutonic rocks. The Mesozoic basement faults formed northeastern-trending fragile fracture zones, that controlled the eruption and distribution of volcanoes and ultimately affected the distribution and morphology of surface volcanic cones (Bai et al., 2005). In May 2017, UNESCO approved Aershan National Geopark as be a world geological park. The geomorphology of the Aershan area is mainly characterized by volcanic cones, lava flows, lava platforms, crater- and volcanic barrier lakes, and hundreds of volcanic hills.

The arid and semiarid areas (35°–50° N and 75°–125° E) in North China make up 30% of the Chinese land and have mean annual precipitation of less than 400 mm. Motianling is located at the transition zone between the semiarid and subhumid areas and is affected by mineral

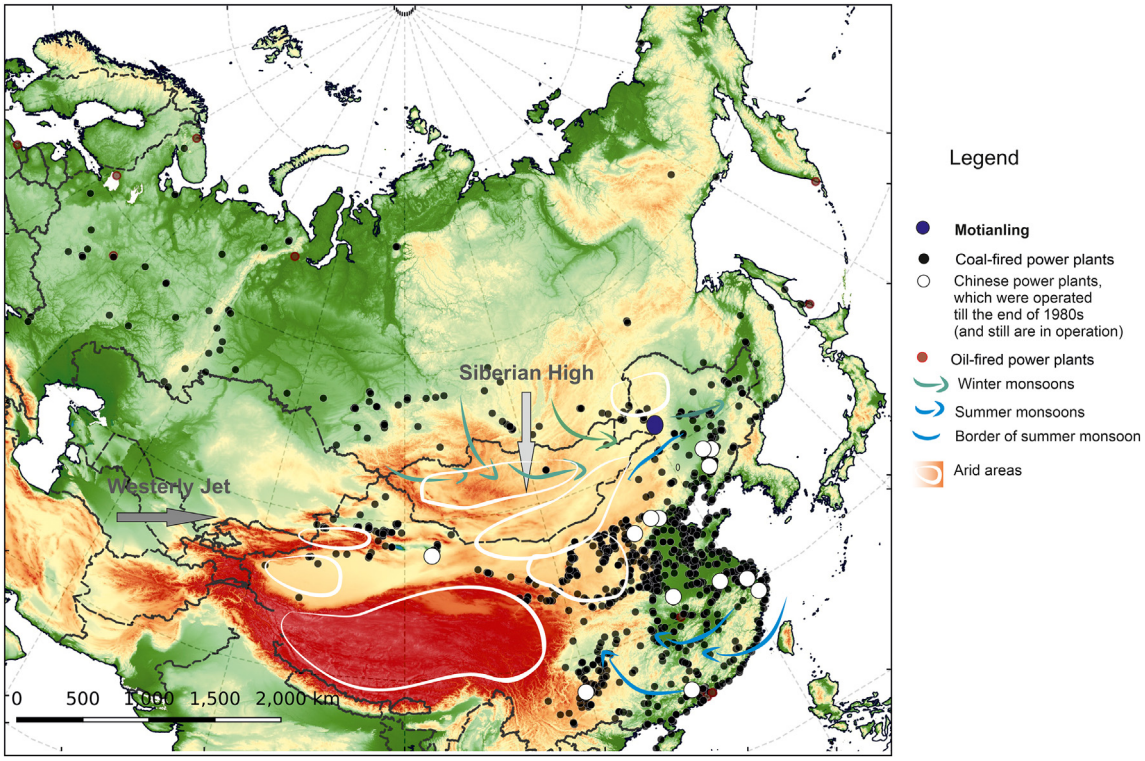

Fig. 1. Map of study site in the global context of Asian industrial development and geographical drivers of dust deposition. Power plants in China and Russia were taken from Global power plants database (2018).

particles carried by the Westerly jet from deserts and drylands (Fig. 1). A cold-temperate climate zone with a terrestrial monsoon dominates in the region, with a mean annual temperature of −2.7 °C and mean annual precipitation of 391 mm (Bao et al., 2012). The major routes through which cold air comes from Siberia in the north to China are the northwestern, northern, and northeastern tracks (Fig. 1). The northwestern cold air intrusion is also an important carrier of eolian dust originating from eastern Mongolia, and the areas affected by this dust storm-inducing system could span eastern Mongolia, Northeast (NE) China, Korea, and Japan (Liu et al., 2003; Jeong et al., 2014).

The peatland analyzed in this study is situated on a north-facing slope of Motianling Mountain. It has an area of approximately 0.50 km^2, and is located at an elevation of about 1712 m a.s.l. The peatland is underlain by the permafrost of the basalt weathering crust. The top part of the peatland predominantly consists of mosses (e.g., *Sphagnum acutifolium* and *Sphagnum girgensohnii*), ericaceous shrubs (e.g., *Ledum palustre* var. *angustum* and *Vaccinium uliginosum*), and a sparse pine cover (*Pinus pumila*) (Bao et al., 2012).

Peat profile from Motianling peatland (MP1) (47°22′13″ N, 120°39′08″ E) was collected in October 2008. Large block (15 × 15 × 64 cm^3) was dug up and then sectioned at 1- or 2-cm intervals to avoid core disruption. All peat samples were stored in polyethylene bags until they were subjected to laboratory analyses. The physical properties of the samples were determined and are described elsewhere (Bao et al., 2010). MP1 was characterized by well-defined minerotrophic peat within a depth range of 46–62 cm, whereas the ash content and bulk density systematically decreased toward the top of the profile thus having more of an ombrotrophic status.

2.2. Chronology

The chronology was assessed using ^{210}Pb and ^{137}Cs according to Bao et al. (2010). Briefly, approximately 1 cm (first 10 cm) and 2 cm-long dry samples were measured for a total ^{210}Pb, ^{226}Ra, and ^{137}Cs using a low-background γ-ray spectrometer equipped with a high-pure Ge semiconductor (ORTEC Instruments Ltd., USA). The measurement was performed at the State Key Laboratory of Lake Science and Environment, Nanjing Institute of Geography and Limnology, Chinese Academy of Sciences. The radioactivity levels of ^{210}Pb were determined based on gamma emissions at 46.5 keV, and that of ^{226}Ra were determined with 295- and 352-keV γ-rays emitted by its daughter nuclide ^{214}Pb after 3 weeks of storage in sealed containers to allow radioactive equilibrium. In the case of ^{137}Cs, the radioactivity levels were measured with a 662-keV photo peak. The absolute efficiency of the detectors was calibrated using the standard sources and sediment samples of known activity provided by the China Institute of Atomic Energy. Counting times of ^{137}Cs and ^{210}Pb were typically in the range of 50,000–86,000 s, which ensured a measurement precision of between ca. ±5% and ± 10% at 95% confidence level. Supported ^{210}Pb in each sample was assumed to be in equilibrium within situ ^{226}Ra, while the activity of unsupported ^{210}Pb was determined from the difference between the total ^{210}Pb and supported ^{210}Pb activity.

2.3. Pb and Pb stable isotopes

The Pb content of MP1 was determined by atomic emission spectroscopy with inductively coupled plasma (Shimadzu Corporation, Japan) after digestion with an acid mixture (HNO_3, $HClO_4$, and HF), and the data are reported elsewhere (Bao et al., 2010). The Pb isotopes were measured by quadrupole inductively coupled plasma mass spectrometry (Q-ICP-MS 7700×; Agilent Technologies, Santa Clara, CA, USA), and the data are reported elsewhere (Bao et al., 2015).

2.4. REE and Sc

Peat samples were dried at 105 °C in a vacuum drier and burned at 550 °C overnight prior to acid digestion in Teflon Savillex® beakers (UAM). First, the samples were treated with 65% HNO_3 and 45% HF for 48 h at 130 °C and then slowly evaporated (55 °C) and treated with oxygen peroxide to remove the organic matter. Finally, the samples were

digested in concentrated HCl for 24 h at 90 °C, evaporated, and dissolved in dilute HNO_3. The total concentrations of Sc and REE were measured by inductively coupled plasma mass spectrometry (UAM). NCS ZC 73018 (Citrus leaves) were used to validate measurements. Details are provided in Suppl. 2. REE concentrations were normalized to post-Archean Australian shale (PAAS; Taylor and McLennan, 1985) as described by Kylander et al. (2007); Zhang et al. (2009); Ferrat et al. (2011, 2012a, 2012b); Fagel et al. (2014); Pratte et al. (2017, 2020).

2.5. Analysis of Nd and Sr isotopes

To trace the sources of atmospheric dust, $^{143}Nd/^{144}Nd$ and $^{87}Sr/^{86}Sr$ values were determined. Briefly, about 300 mg of peat powder was burned at 550 °C overnight, and the ash obtained was dissolved on a hot plate (~100 °C for 3 days) in closed perfluoroalkoxy vials using a mixture of concentrated hydrofluoric acid and nitric acid (4:1). Miniaturized chromatographic techniques described by Pin et al. (1994) were utilized for the separation of Nd and Sr, with some modifications in column size and reagent concentrations according to Dopieralska (2003). Strontium was loaded with a $TaCl_5$ activator on a single Re filament, whereas Nd was measured in a Re double-filament configuration. The instrumental drift was controlled by the AMES standard and NBS 987. The εNd value was calculated using the following standard formula: $\varepsilon Nd\ sample = (^{143}Nd/^{144}Nd\ sample - 0.512638 / 0.512638) * 10000$, where 0.512638 is the chondritic uniform reservoir. Isotopic ratios were measured by thermal ionization mass spectrometry (Finnigan MAT-261; UAM Poznań).

2.6. Mineralogy

Major crystalline inorganic phases in the peat samples were identified using X-ray powder diffraction (XRD). The samples were subjected to thermal combustion at 495 °C to efficiently remove organic matter (Sjöström et al., 2019). Additionally, high-ash samples were analyzed without any pretreatment, and selected samples were combusted at 550 °C to identify clay minerals. Analyses were performed at the University of Silesia using a PANalytical X'Pert PRO PW 3040/60 X-ray diffractometer equipped with an Ni-filtered Co Kα source radiation (λ = 1.789010 Å) and X'Celerator detector. The content of mineral phases was determined using the Rietveld method. The variable degree of structural order/disorder (illite) and differences in peak position and intensity (chlorite) observed for clay minerals between row and thermally treated samples made the results semiquantitative.

Individual dust particles were analyzed using scanning electron microscopy (SEM; University of Silesia). Briefly, a small portion of each sample was mounted on an aluminum specimen stub and coated with carbon before the examination. A backscattered electron detector of SEM-FEI Quanta 250 coupled to an energy-dispersive X-ray analyzing system was used at an accelerating voltage of 15 kV and a working distance of 10 mm.

3. Results

3.1. Chronology

The chronology data are provided elsewhere (Bao et al., 2010, 2012). In this study, we briefly stated that the unsupported ^{210}Pb activity exponentially decreased with depth and became constant at depths ranging from 58 to 64 cm, which is consistent with the equilibrium depth of total ^{210}Pb and supported ^{210}Pb. According to the age-depth relationships of peat cores derived based on the CRS model, the sediments in the MP1 spanned a period of about 135 years.

3.2. Peat mineralogy

The results showed the presence of common rock-forming silicate and aluminosilicates: quartz, feldspars (e.g., albite and microcline), clay minerals (e.g., illite, chlorite), one mineral from the pyroxene group (augite), and an amphibole (hornblende). In addition, a small amount of hematite was identified in two bottom samples. The occurrence of ~12% of augite, with a decreasing content toward the top of the peat profile, was used as a criterion to differentiate between the bottom (46–64 cm) and high-ash (36–73%) minerotrophic peat and the upper layers with a lower ash content (5.3–19%). Augite was found below the detection limit, starting from 46 cm.

Clay minerals were present throughout the profile. Illite was found to be the most abundant (up to 30%) in the bottom and uppermost samples, with a lower content (10–15%) at a depth interval of 25–46 cm. In contrast to illite, which is thermally stable up to 550 °C (Sjöström et al., 2019), chlorite, present in low amounts (1–4%), was confirmed by comparing the thermally pretreated samples with untreated ones. The 001 and 002 peaks of chlorite (Fe clinochlore and/or chamosite) occurred at 14.05–14.25 Å and 7.06–7.10 Å, respectively, for untreated samples and samples burnt at 495 °C. Further thermal treatment at 550 °C causes a shift in the 001 peak to 13.86–13.98 Å and destruction of the 002 peak (Suppl. 1), which is in accordance with a process observed for pure Mg chamosite by Lempart et al. (2018). The occurrence of kaolinite, in a meager amount, could not be excluded as the 001 peak of the mineral that appeared at 7.18 Å also diminished due to thermal treatment. A small peak at 8.40–8.42 Å, interpreted as 110 of hornblende, was seen in all samples (Suppl. 1). Quartz and feldspars were the minerals predominantly found, which contributed equally to the crystalline part determined by XRD.

SEM was utilized to determine the amorphous constituents, weathering state of mineral particles, and mutual relations among the inorganic particles. Firstly, no formation of secondary mineral phases was observed in both the minerotrophic and ombrotrophic parts of the profile. Secondly, the aluminosilicates showed no weathering features characteristic of dissolution in a peat bog (Franzén, 2006). An example of euhedral unweathered augite crystal aggregate is shown in Fig. 2.

SEM analyses revealed the presence of two types of aluminosilicate glass particles. Large volcanic glass shards (up to 200 μm) were observed only in the high-ash part of the profile (Fig. 2). Anthropogenic spheroidal aluminosilicate particles (SAP), in a small number per sample, were observed starting from 36 cm upward. These particles had a much higher Al/Si ratio than the volcanic glass and were extremely small, measuring between 0.3 and 4.8 μm, with a mean diameter of 1.5 μm (n = 45). Single porous and rounded but irregular aluminosilicate particles appeared in the uppermost part of the profile, which were slightly larger than SAP (Fig. 2). Tar spherules with a diameter of ~10 μm were identified at a depth of 36–40 cm (Fig. 2).

Aggregates of clay minerals containing feldspars or quartz were also observed, which are characteristic of the ombrotrophic part of the profile. They were relatively large (20–60 μm) and irregular with rounded edges. An example of an aggregate composed of clay minerals, feldspars, TiO_2 particles, and Fe(hydro)oxide is shown in Fig. 2.

3.3. REE patterns of distribution

The overall concentrations of REE and the normalized REE values are reported in the supplementary material (Suppl. 2). Like ash content, two parts were established: one with an enhanced concentration from a depth of 64 to 46 cm (1872–1946 CE) and one with a diminished concentration from 46 cm to upward (1954–2004 CE). Total REE concentrations ($\sum$REE) in the minerotrophic layer ranged between 31 and 67 $mg \cdot kg^{-1}$, with the highest concentrations found at 32–34 cm (1928 CE). The scandium content in the minerotrophic part of the profile varied from 1.85 to 4.95 $mg \cdot kg^{-1}$, and the values were higher than those determined for the oligotrophic part of the profile (0.42–1.33 $mg \cdot kg^{-1}$).

Based on the PAAS-normalized REE patterns (Fig. 3 and Suppl. 2), the profile was divided into slightly LREE-enriched layers and HREE-enriched layers. The two most bottom layers (62–64 cm, 1872 CE;

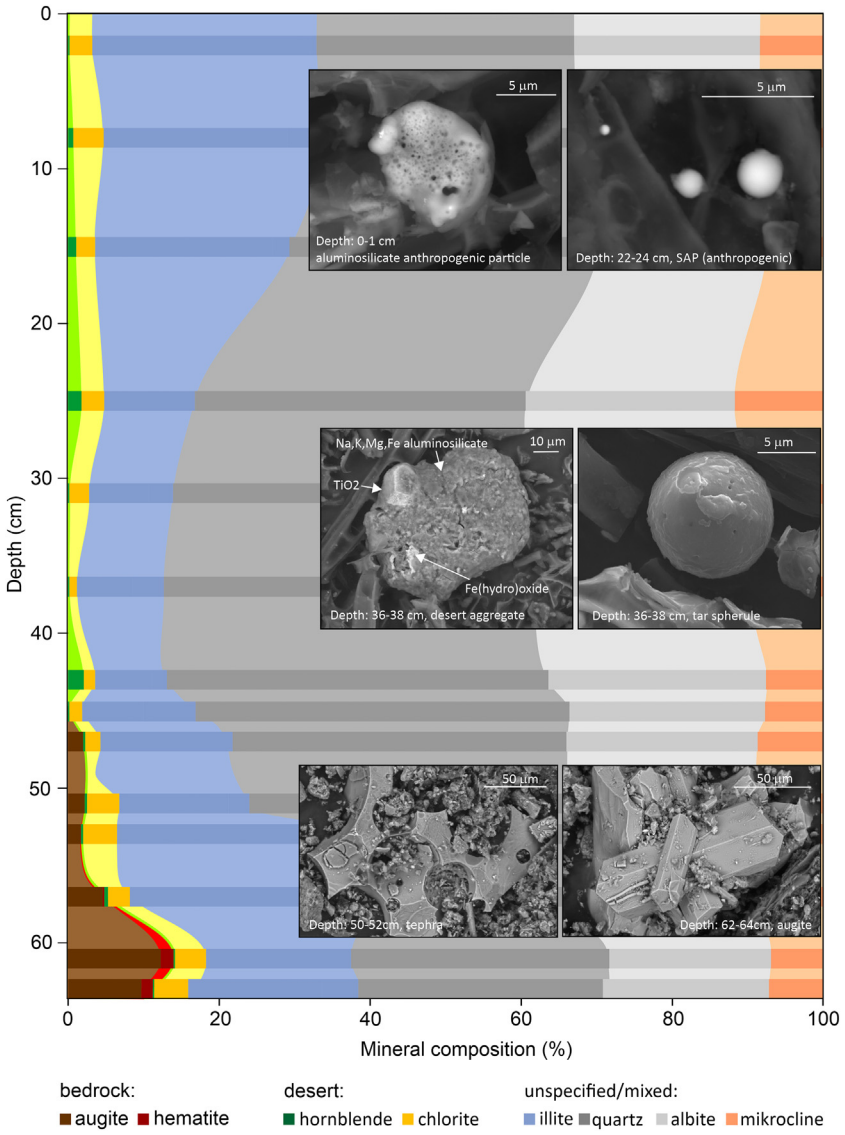

Fig. 2. Mineral composition of the peat core (XRD-analyzed samples are indicated in the darker colour shade); the source of the minerals (bedrock, desert, mixed) is specified. The XRD mineral composition is accompanied by SEM images of particles representative of the peat. (For interpretation of the references to colour in this figure legend, the reader is referred to the web version of this article.)

62–60 cm, 1891 CE) showed higher HREE values, and layers dated from the years 1928 to 1932 (50–54 cm) showed slightly lower LREE values (Fig. 3). All the peat layers exhibited weak Eu enrichment, except for samples dated 1977 (26–28 cm) and 1988 (14–16 cm), where PAAS-normalized Gd value was higher than the Eu value. The topmost layer (2004 CE) was characterized by higher ∑REE compared to other layers within the ombrotrophic part.

Dust flux (g $m^{-2}y^{-1}$) was calculated according to the formula: PAAS-normalized ∑REE x bulk density x peat accumulation rate (as described in Shotyk, 2002; Pratte et al., 2017) separately for minerotrophic and ombrotrophic parts of the profile (Fig. 4). It is important to note that two samples within the depth of 40–44 cm (comp. Suppl. 2) were excluded from the final interpretation because the dust flux calculated for this layer was unrealistically exaggerated compared to row concentrations (Suppl. 2). The calculations were affected by a twofold increase in bulk density, which might be probably due to internal processes (high water level fluctuations) causing higher decomposition, resulting in higher bulk density. It is proved elsewhere that peatland can restore and, after excluding the disturbed peat parts, it is still possible to make a complete interpretation (Fiałkiewicz-Kozieł et al., 2014, 2018; Milecka et al., 2017). In the minerotrophic part, dust flux increased exponentially from 5.3 to 38,8 $g \cdot m^{-2} \cdot y^{-1}$ reaching the maximum in 1928 CE, followed by an exponential decrease to 8.7 $g \cdot m^{-2} \cdot y^{-1}$. In turn, in the ombrotrophic part, the highest dust flux was distinguished in 1960 CE (12.8 $g \cdot m^{-2} \cdot y^{-1}$), and from 1964 to 2004, there were smaller seasonal increases in the value.

3.4. Radiogenic isotope systems (Pb, Nd, and Sr)

From the Pb isotope ratios of all the investigated samples, regarding the function of age and depth (Table 1 and Suppl. 1), we observed the evolution from more radiogenic to less radiogenic signature of $^{206}Pb/^{207}Pb$ and from less radiogenic to more radiogenic signature of $^{208}Pb/^{206}Pb$ toward the top of the profile. In the minerotrophic part, the isotopic signature of $^{206}Pb/^{207}Pb$ ranged between 1.1941 and 1.1854, while that of $^{208}Pb/^{206}Pb$ from 2.0783 to 2.0813. In the ombrotrophic part, an exponential decrease in the signature of $^{206}Pb/^{207}Pb$ from 1.1868 to 1.1584 and an increase in the signature of $^{208}Pb/^{206}Pb$ from 2.0779 to 2.1156 were established.

Seven samples were measured for Nd and Sr isotopic differentiation (Table 1). In the minerotrophic part, the $^{143}Nd/^{144}Nd$ signature ranged from 0.512260 to 0.512471, εNd from −3.258 to −7.374, and

$^{87}Sr/^{86}Sr$ signature from 0.708880 to 0.710524. In the ombrotrophic part, the $^{143}Nd/^{144}Nd$ signature varied from 0.512222 to 0.512369. A shift in εNd from the value of −5.247 to −8.115 was observed, and the values of $^{87}Sr/^{86}Sr$ signature ranged from 0.710428 to 0.710728.

4. Discussion

4.1. Bedrock–peat interaction as a driver of enhanced trophy

Motianling peatland lies on quaternary volcanic bedrock, which significantly influenced the development and geochemical composition of the bottom part of the peat confirmed by the occurrence of fresh tephra shards together with augite and hematite due to the redeposition of local volcanic ash (Fig. 2). It can be explained by the fact that during the initial stages of peatland formation, water input and mineral matter were mainly received from surface runoff and slope wash driven by seasonal climatic variations (Bai et al., 2005; Bao et al., 2010, 2012) in addition to the atmospheric water and dust deposition.

The peatland is in the humid, cold climate zone, which allows the stabilization of the bedrock by native vegetation, resulting in a gradual reduction in local dust emission (Le Roux and Shotyk, 2006), promoting the development of ombrotrophic peat. Based on geomorphology, ash, and mineral content, the distinguished evolution of peatland toward ombrotrophic status and hydrological isolation from surface water runoff are confirmed by the lack of the volcanogenic constituents (e.g., augite, hematite, and volcanic glass) in the ombrotrophic part of the profile and by increasing content of particles originating from deserts. From 46 cm upward, the deposit is exclusively fed by air-deposited mineral matter.

In addition, it seems that postdepositional processes are insignificant in the minerotrophic part, as primary aluminosilicate minerals were found to dominate in the inorganic peat fraction, while no secondary phases or dissolution features on mineral surfaces were observed.

In agreement with the steady-state mineralogy, the REE pattern appears to remain unaffected by the peatland conditions (e.g., redox potential, pH) (Figs. 3 and 4). The calculated PAAS-normalized Ce values (minerotrophic: 1.005–1.08; ombrotrophic: 0.947–1.000) were almost uniform throughout the whole profile (Fig. 4 and Suppl. 2). It is known that the valence of cerium might change from Ce^{3+} to Ce^{4+} during the low-temperature oxidation process (Kylander et al., 2007; Davranche et al., 2017), which possibly might induce mobilization in peat. Different Eu and Ce distribution patterns and other individual REE profiles due to oxidation were observed in a Swiss peatland (Krachler et al., 2003). The comparable Ce values through the Motianling profile indicate lack of the redox effect on the valence of Ce.

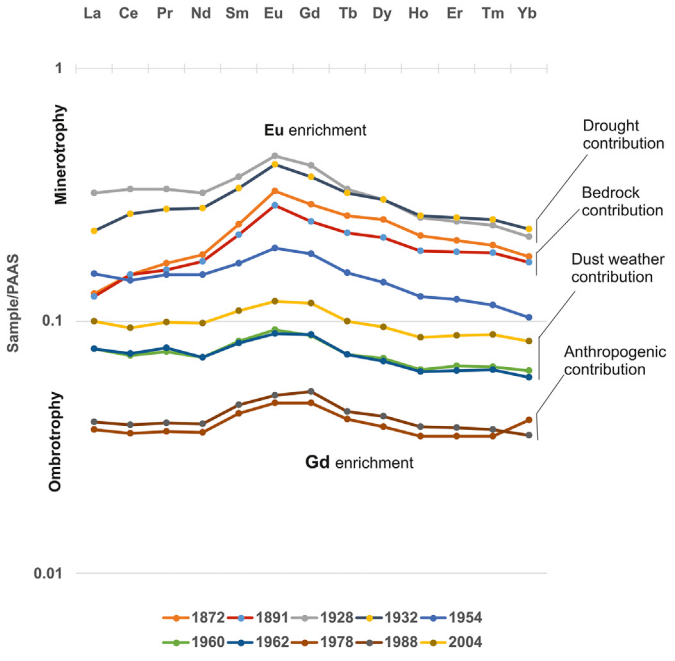

Fig. 3. PAAS normalized pattern of REE distribution in selected peat layers referred to minerotrophic and ombrotrophic part of profile.

The two most bottom layers dated 1872 CE and 1890 are characterized by the lowest PAAS La/Yb ratio (0.7; Fig. 4), indicating the HREE enrichment. Accordingly, the [Eu/Eu*] values (1.22–1.24) of the two bottoms layers (Fig. 4), were distinctly higher compared to external sources, including Chinese loess plateau (0.91–1.05), Chinese deserts (0.95–1.00), and Tibetan soils (0.94–0.99; Ferrat et al., 2011). Conversely, the values are very similar to the REE signature of basaltic rocks, characterized by positive $[Eu/Eu^*]_{PAAS} = 1.29–1.56$ (Schettler et al., 2006; Pratte et al., 2020). The εNd value (−3.26) was like quaternary lava values (Nakano et al., 2004) (Fig. 5). The values of Pb isotopes ($^{206}Pb/^{207}Pb$: 1.194) were typical for natural signature (Novak et al., 2003; Sun and Zhu, 2010; Bory et al., 2014; Bao et al., 2015). These results—combination of the highest Eu/Eu*, high εNd, low La/Yb, and the occurrence of augite and hematite (Fig. 2)—prove the prevailing impact of the local geology on peat geochemistry.

4.2. Delivery of desert-originated particles

Northern China and Mongolia are among the most important sources of dust, which deliver permanently with seasonal variations in winter temperature and cyclone frequency (Zhang et al., 1997; Sun et al., 2001; Qian et al., 2002; Nakano et al., 2005; Wang et al., 2011). Gobi-type deserts, sandy deserts and piedmont alluvial fan are also important contributors to Asian dust storms (Wang et al., 2015). In Motianling, the mineral particles are observed through the whole profile (Fig. 2), confirming the contribution of arid areas to the inorganic matter of peat. Chlorite and hornblende (dark amphibole) identified by XRD pointed out dust delivery from outside the Great Hinggan Mountains. Studies on recent dust storms have confirmed that large (<5–60 μm) particles of clay-coated quartz, feldspars, and clay agglomerates are transported over 2000 km from the Gobi Desert in the east direction. Dust originating from Gobi comprises illite, chlorite, quartz, and feldspars, as well as a smaller amount of amphibole (Jeong et al., 2014). Still, it is important to add that quartz, feldspars, and clay minerals are significant constituents of many arid areas (Ferrat et al., 2011), so the most distinguishable feature of Gobi signature is the occurrence of hornblende.

A comparison of the PAAS-normalized ratio of REE (Fig. 3) and La/Yb ratio, Eu/Eu* anomaly, and Y/TbPAAS with the graph of dust flux generated based on PAAS-normalized ∑REE (Fig. 4) allows to distinguish the episodes of enhanced mineral matter supply from deserts in 1928 CE (52–54 cm). The evidence obtained is also compatible with historical data. The time interval 1925–1940 was characterized by dry or even drought events in China (Liu et al., 2003). In the last 120 years, 1920s was the driest decade in northern China (Wang et al., 2004; Liang et al., 2006). Severe drought episodes were also detected in Mongolia (Liang et al., 2003, 2006).

In the ombrotrophic part, the highest climatically driven dust deposition was distinguished in 1960 (36–38 cm) with smaller peaks in the upper parts of the profile. The marked shifts are similar to the 50-year record of dust storm and dust weather for China (Qian et al., 2002; Liu et al., 2003), which indicates the reliability of the determined dust flux and close correlation with climatic factors (Fig. 4). The top 2004 sample has a different REE pattern comparing to the lower parts of the ombrotrophic part of the profile (Fig. 3). The highest number of anthropogenic particles together with a large amount of fine fraction of geogenic particles indicates the increasing role of industry as well as the enhanced delivery of naturally originated mineral matter. The severe dust storms, covering the neighboring Asian countries as well as North America, have been noticed many times (Nakano et al., 2005).

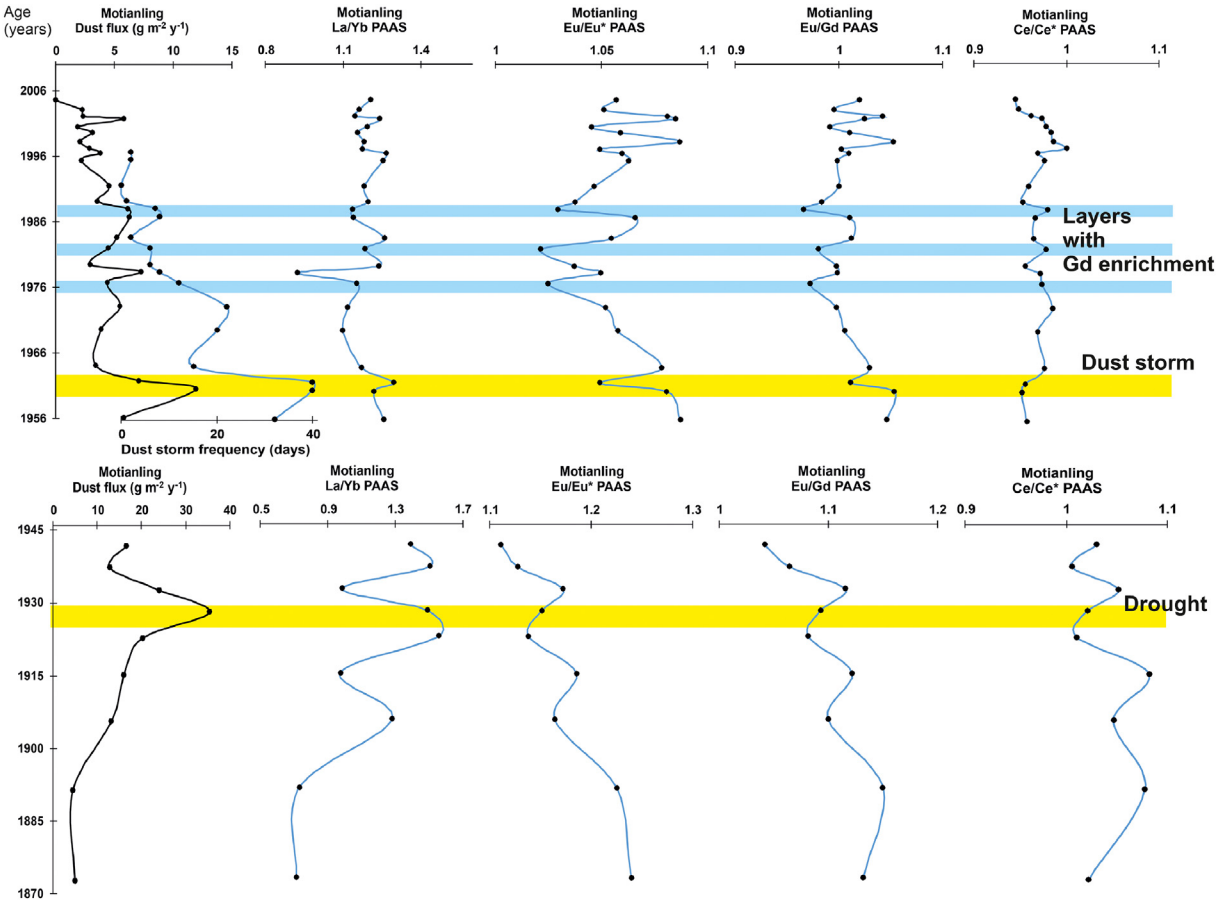

Fig. 4. ∑REE-based dust flux and selected REE ratios vs. age as well as dust storm changes in Northern China based on Liu et al. (2003).

While the delivery of the natural particles is obvious, two distinct groups of samples (1 group: AD1872, 1928, 1932, 1960; and 2 group: AD1954; 1962; 2004) differing with Nd and Sr isotopic signature are observed (Fig. 5). North of Northern China to Mongolia, Southern Gobi, and Loess Plateau as well as Taklimakan desert, are characterized by a wide variation in $^{87}Sr/^{86}Sr$ ratios (0.71105–0.73658) and εNd values (−28.7 to −4.0) and can be divided into distinct regions based on the different isotopic signatures (Nakano et al., 2004). εNd values and $^{87}Sr/^{86}Sr$ signature of samples of the first group are representative of eolian deposition similar to Northern Gobi and northern Chinese deserts (Fig. 5) and confirm, that Motianling, located at the Mongolia–China border, is exposed to dust from western arid areas due to prevailing northwesterly movement of air mass (Fig. 1; Sun et al., 2001; Bao et al., 2012; Ferrat et al., 2012a, 2012b; Pratte et al., 2020; Zhang et al., 2021). At the same time, they are distinct from the Southern Gobi (Badain Jaran, Tengger, Ulan Buh, Hobq, Mu Us), Chinese loess plateau, Taklimakan, and Tibetan soils (Fig. 5). Taklimakan can additionally be excluded due to the prevailing easterly and north-easterly wind direction. The dust from there is lofted up to 5000 m and moves north and northwest (Sun et al., 2002; Nakano et al., 2004).

The second group represents a mixed pattern (desert and human impact) and is difficult to define isotopically using Nd and Sr. Regarding Pb isotopes, $^{206}Pb/^{207}Pb$ and $^{208}Pb/^{206}Pb$ of eolian dust from Taklimakan (1.19–1.203; 2.066–2.08), Inner Mongolia (1.200; 2.076), loess samples (1.198–1.206; 2.070), and quaternary basalts from Heilongjiang (1.09–1.15; 2.13–2.19) reported in previous studies (Peng et al., 1986; Bi et al., 2017; Schleicher et al., 2020) are distinct from the peat isotopic composition (Fig. 6 and Suppl. 2), indicating an additional source of the isotopes.

4.3. Disequilibrium between natural and anthropogenic sources of dust in ombrotrophic part of peat deposit

While the overall pattern of dust distribution in the ombrotrophic part of Motianling peatland is comparable with drought events, the geochemical signature of the topmost samples was found to be different, indicating an additional anthropogenic source of elements (comp. Figs. 2, 4, and 5).

Combining the mineralogical and isotopic results, the most unequivocal signal linked to industrial activity was detected in 1964. During that

Table 1
$^{87}Sr/^{86}Sr$, $^{143}Nd/^{144}Nd$, εNd and modelled age for selected samples.

Sample	$^{143}Nd/^{144}Nd_{(0)}$	2σ	$^{87}Sr/^{86}Sr_{(0)}$	2σ	εNd	206Pb/207Pb	Modelled age
MP 0–1	0.512222	±0.000015	0.710728	±0.000010	−8.114888089	1.158	2004
MP 34–36	0.512258	±0.000012	0.710559	±0.000012	−7.412638158	1.179	1962
MP 36–38	0.512369	±0.000014	0.710428	±0.000009	−5.247367538	1.182	1960
MP 42–44	0.512260	±0.000013	0.709885	±0.000010	−7.373624273	1.187	1954
MP 50–52	0.512386	±0.000010	0.710524	±0.000012	−4.915749515	1.192	1932
MP 52–54	0.512419	±0.000012	0.710355	±0.000011	−4.272020412	1.192	1928
MP 62–64	0.512471	±0.000011	0.708880	±0.000010	−3.257659401	1.194	1872

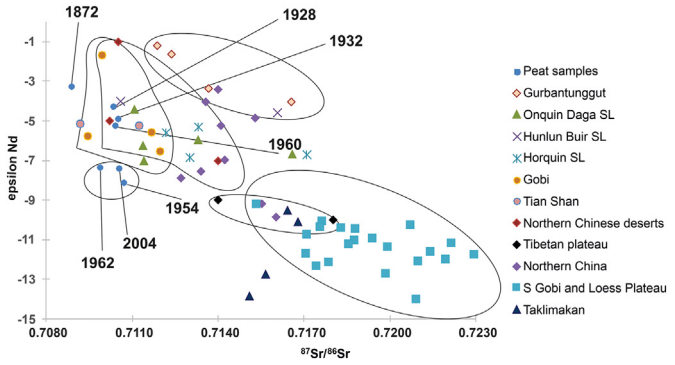

Fig. 5. $^{87}Sr/^{86}Sr$ vs. εNd values of peat samples and potential sources of natural dust: Gurbantunggut Desert, Onqin Daga Sandy Land, Hunlun Buir Sandy Land, Horqin Sandy Land, (Chen et al., 2007); Gobi (Chen et al., 2007; Biscaye et al., 1997); Tian Shan (Liu et al., 1994); Northern Chinese deserts, Tibetan Plateau (Li et al., 2009), Southern Gobi, Chinese Loess Plateau, Taklimakan (Nakano et al., 2004).

period, the first appearance of fly-ash SAP, produced during high-temperature processes in coal-fired power plants, was observed. Nonetheless, the SAP were very small (1.5 μm), compared to the particles in other peatlands (located in Europe and Western Siberia), measured using the same methodology (Smieja-Król and Fiałkiewicz-Kozieł, 2014; Fiałkiewicz-Kozieł et al., 2016, 2020). The appearance of SAP was followed by a decrease in Pb isotopic signature from 1.194 in 1872 to 1.167 in 1964. The shift, also described in other case studies from Europe (Shotyk et al., 1997; Shotyk et al., 1998a, 1998b, 2003; De Vleeschouwer et al., 2009; Fiałkiewicz-Kozieł et al., 2018, 2020) and America (Pratte et al., 2013; Drexler et al., 2016; Shotyk et al., 2016), confirms the human impact. While the anthropogenic influence is evident, the source of the anthropogenic signatures is not clear.

From the late 1970s, China saw an industrial revolution (Cheng and Hu, 2010; Wan et al., 2020); however, the first grade-firing boilers came into use in Tianjin in NE China, followed by two other power plants built in Harbin, only in 1905 (IEEE-PES, 2008). No SAP linked to early power plant activity (before 1964) were detected in the peat profile. Such large, porous aluminosilicates were determined in mountain peatland located in central Europe (Fiałkiewicz-Kozieł et al., 2020). The Pb isotopic composition of Motianling, associated with the acceleration of Chinese industries, displays a dissimilarity to the coal deposits, ores, and gasoline signatures of NE China (Fig. 6; Bi et al., 2017). A detailed

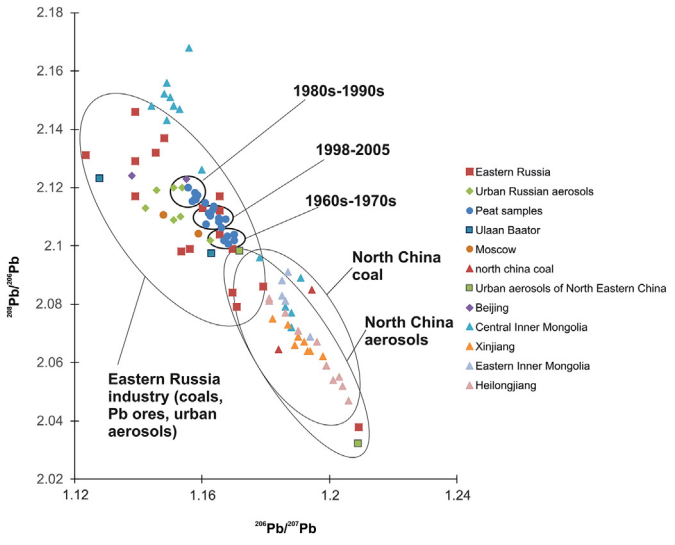

Fig. 6. $^{206}Pb/^{207}Pb$ vs. $^{208}Pb/^{206}Pb$ in peat samples and anthropogenic sources. Northern Chinese coals were taken from Bi et al. (2017); Bejing, Ulaan Baator, Moscow values – Bollhöfer and Rosman, 2001; Russian sources - Mukai et al., 2001.

analysis of winds parameters and location of Motianling relative to main industrial centers, showed that in 1960s and 1970s only three power plants existed in the southeastern part of Heilongjiang (Fig. 1; Suppl. 3), in cities affected by more monsoon climate regime and domination of winds from south and west. The prevalence of western winds and the northern boundary of summer monsoon below the Motianling location sufficiently block the transport of pollutants from the industries located in the southern and eastern part of China (comp. Fig. 1). This allowed the assumption that Motianling received trace elements via transboundary transport, and sources other than Chinese might be involved before the Chinese industrial boost. The biplot of $^{206}Pb/^{207}Pb$ versus $^{208}Pb/^{206}Pb$ (Fig. 6) suggests the transboundary transport of anthropogenic particles from the north direction (Fig. 1 and Suppl. 2). Delivery from the southern part of Asian Russia during the 1970s and 1980s is more possible due to the tenfold higher number of power plants and other industrial points compared to China at that time (Suppl. 3 and Fig. 6). According to accessible data, there was an acceleration in Chinese industrial activities after 1990, when power plants started to mushroom in the whole country (Global Power Plants Database, 2018; Suppl. 3). The topmost layer of the peatland exhibits a higher Pb concentration, indicating a rapid increase of power plants in the northwestern and northeastern parts of China (Suppl. 2). However, a low SAP concentration confirms the usage of novel technology and emission control systems in modern power plants (Fig. 2 and Suppl. 3).

Despite the similarity between the dust flux of the peatland in this study and the typical Asian dust weather fluctuations, the distribution pattern of REE revealed a slight increase in PAAS-normalized Gd concentrations during the period 1978–1988, which could be due to the industrial contribution to the REE composition of peat (Figs. 3 and 4). Gd enrichment is observed only in the ombrotrophic part of peat, when the contribution of desert dust is much lesser, and the lack of enrichment in the other peat layers of Motianling might be attributed to the excessive natural dust input. China is the most important producer of REE, and the largest ore deposit, Bayan Obo, is in the west of Inner Mongolia (Deng et al., 2017). However, research conducted near the mine reveals no Gd enrichment, and there is no evidence supporting the influence of mining and processing on the atmospheric deposition of Gd in Motianling. Another explanation is coal combustion with a defined Gd anomaly, which has been established for Chinese and Far Eastern Russian coals (Dai et al., 2016). Such Gd enrichment has been observed in European peatlands that are located near industrial centers emitting coal-based particles (comp. Fagel et al., 2014; Fiałkiewicz-Kozieł et al., 2020). However, this is in contradiction with the deficient number of fly-ash particles in the peat and needs further research.

5. Conclusions

Motianling peatland exhibits two phases of geochemical evolution, which are strongly related to trophy status and age. REE and isotope analyses confirmed that westerly-carried particles from northern China and Mongolia are a prevailing source of dust deposition in the Chinese mountain peatland. Dust flux mirrors a dramatic increase during drought events. The anthropogenic activity in the peatland is manifested by a decrease in $^{206}Pb/^{207}Pb$ and εNd values. Nonetheless, the human impact is masked by natural desert dust, which makes the distinction between the two origins more difficult. The impact of coal-fired power plants is reflected by the occurrence of a few micrometer-sized fly-ash SAP, which remain small throughout the profile and points out the prevalence of long-range transport.

In the light of the industrial database and the Pb isotopic signature, it can be concluded that the main contributor of anthropogenic fraction till the late 1980s might be the industrial centers located in the southern part of Asian Russia, near the Chinese border. This is also supported by the domination of western and northern wind direction. However, substantial development in the northern part of China also contributes to the anthropogenic delivery of elements to the peatland.

During limited transportation of desert particles, a slight Gd enrichment is observed, which might be due to the combustion of coal with typical Gd anomaly.

Supplementary data to this article can be found online at https://doi.org/10.1016/j.scitotenv.2021.150481.

CRediT authorship contribution statement

Barbara Fiałkiewicz-Kozieł: conceptualization, sample preparation for REE analysis, calculations (normalisations, accumulations, dust flux), interpretation of REE, Pb, Sr and Nd isotopes, draft writing and revision, visualization of results (Graphical abstract and Figs. 1, 3, 4, 5, 6, Table 1, Supl. 2, 3), funding acquisition; **Beata Smieja-Król:** mineralogical analyses and their interpretation, preparation of Fig. 2, and Suppl. 1; **Kunshan Bao:** providing of peat material, age depth model, Pb isotopes, funding acquisition.

Declaration of competing interest

The authors declare that they have no known competing financial interests or personal relationships that could have appeared to influence the work reported in this paper.

Acknowledgements

The research was supported by grant no. 2017/27/B/ST10/00428 from National Science Centre, Poland, and grant no. 41971113 from National Natural Science Foundation of China. Marcin Siepak and Jolanta Dopieralska are thanked for geochemical measurements. Tomasz Krzykawski is thanked to conduct XRD analyses. Jarosław Jasiewicz is thanked for help with the preparation of Fig. 1.

References

Bai, Z., Tian, M., Wu, F., Xu, D., Li, T., 2005. Yanshan, Gaoshan – two active volcanoes of the volcanic cluster in Aershan, Inner Mongolia. Earthq. Res. China 19 (4), 402–408.

Bao, K., Xia, W., Lu, X., Wang, G., 2010. Recent atmospheric lead deposition recorded in an ombrotrophic peat bog of great Hinggan Mountains, Northeast China, from 210Pb and 137Cs dating. J. Environ. Radioact. 101, 773–779.

Bao, K., Xing, W., Yu, X., Zhao, H., McLaughlin, N., Lu, X., Wang, G., 2012. Recent atmospheric dust deposition in an ombrotrophic peat bog in great Hinggan Mountain, Northeast China. Sci. Total Environ. 431, 33–45.

Bao, K., Shen, J., Wang, G., Le Roux, G., 2015. Atmospheric deposition history of trace metals and metalloids for the last 200 years recorded by three peat cores in Great Hinggan Mountain, Northeast China. Atmosphere 6 (3), 380–409.

Bao, K., Wang, G., Jia, L., Xing, W., 2019. Anthropogenic impacts in the Changbai Mountain region of NE China over the last 150 years: geochemical records of peat and altitude effects. Environ. Sci. Pollut. Res. 26 (8), 7512–7524.

Bi, X.Y., Li, Z.G., Wang, S.X., Zhang, L., Xu, R., Liu, J.L., Yang, H.M., Guo, M.Z., 2017. Lead isotopic compositions of selected coals, Pb/Zn ores and fuels in China and the application for source tracing. Environ. Sci. Technol. 51 (22), 13502–13508.

Bindler, R., 2006. Mired in the past - looking to the future: geochemistry of peat and the analysis of past environmental changes. Glob. Planet. Chang. 53 (4), 209–221.

Biscaye, P.E., Grousset, F.E., Revel, M., Van der Gaast, S., Zielinski, G.A., Vaars, A., Kukla, G., 1997. Asian provenance of glacial dust (stage 2) in the Greenland Ice Sheet Project 2 Ice Core, Summit, Greenland. J. Geophys. Res. Oceans 102 (C12), 26765–26781.

Bollhöfer, A., Rosman, K.J.R., 2001. Isotopic source signatures for atmospheric lead: the northern hemisphere. Geochim. Cosmochim. Acta 65 (11), 1727–1740.

Bory, A.J.M., Biscaye, P.E., Grousset, F.E., 2003. Two distinct seasonal asian source regions for mineral dust deposited in Greenland (NorthGRIP). Geophys. Res. Lett. 30, 1167.

Bory, A.J.M., Abouchami, W., Galer, S.J.G., Svensson, A., Christensen, J.N., Biscaye, P.E.A., 2014. Chinese imprint in insoluble pollutants recently deposited in Central Greenland as indicated by lead isotopes. Environ. Sci. Technol. 48, 1451–1457.

Chen, J., Li, G.J., Yang, J.D., Rao, W.B., Lu, H.Y., Balsam, W., Sun, Y.B., Ji, J.F., 2007. Nd and sr isotopic characteristics of chinese deserts: implications for the provenances of asian dust. Geochim. Cosmochim. Acta 71, 3904–3914.

Cheng, H., Hu, Y., 2010. Lead (Pb) isotopic fingerprinting and its applications in lead pollution studies in China: a review. Environ. Pollut. 158, 1134–1146.

Cong, J., Gao, C., Han, D., Liu, H., Wang, G., 2019. History metal (Pb, zn, and Cu) deposition and pb isotope variability in multiple peatland sites in the northern great Hinggan Mountains, Northeast China. Environ. Sci. Pollut. Res. 26 (21), 21784–21796.

Dai, S., Graham, I.T., Ward, C.R., 2016. A review of anomalous rare earth elements and yttrium in coal. Int. J. Geol. 159, 82–95.

Davranche, M., Gruau, G., Dia, A., Le Coz-Bouhnik, M., Marsac, R., Pédrot, M., Pourret, O., 2016. Chapter 7. Rare Earth Elements in wetlands. In: Rinklebe, J., Knox, A.S., Paller, M. (Eds.), Trace Elements in Waterlogged Soils and Sediments. Taylor & Francis Group/CRC Press, pp. 135–162.

DeBell, L.J., Vozzella, M., Talbot, R.W., Dibb, J.E., 2004. Asian dust storm events of spring 2001 and associated pollutants observed in New England by the Atmospheric Investigation, Regional Modeling, Analysis and Prediction (AIRMAP) monitoring network. J. Geophys. Res. Atmos. 109.

De Vleeschouwer, F., Fagel, N., Cheburkin, A., Pazdur, A., Sikorski, J., Mattielli, N., Renson, V., Fialkiewicz, B., Piotrowska, N., Le Roux, G., 2009. Anthropogenic impacts in North Poland over the last 1300 years - a record of pb, zn, cu, ni and S in an ombrotrophic peat bog. Sci. Total Environ. 407 (21), 5674–5684.

Deng, M., Xu, C., Song, W.L., Tang, H.Y., Liu, Y., Zhang, Q., Zhou, Y., Feng, M., Wei, C.W., 2017. REE mineralization in the bayan obo deposit, China: evidence from mineral paragenesis. Ore Geol. Rev. 91, 100–109.

Dopieralska, J., 2003. Neodymium Isotopic Composition of Conodonts as a Palaeoceanographic Proxy in the Variscan Oceanic System. Justus-Liebig-University, Giessen, p. 111 Ph.D. thesis.

Drexler, J.Z., Alpers, C.N., Neymark, L.A., Paces, J.B., Taylor, H.E., Fuller, C.C., 2016. A millennial-scale record of Pb and Hg contamination in peatlands of the Sacramento-San Joaquin Delta of California, USA. Sci. Total Environ. 551-552, 738–751.

Erel, Y., Veron, A., Halicz, L., 1997. Tracing the transport of anthropogenic lead in the atmosphere and in soils using isotopic ratios. Geochim. Cosmochim. Acta 61 (21), 4495–4505.

Fagel, N., Allan, M., Le Roux, G., Mattielli, N., Piotrowska, N., Sikorski, J., 2014. Deciphering human-climate interactions in an ombrotrophic peat record: REE, nd and pb isotope signatures of dust supplies over the last 2500 years (Misten bog, Belgium). Geochim. Cosmochim. Acta 135, 288–306.

Ferrat, M., Weiss, D.J., Strekopytov, S., Dong, S., Chen, H., Najorka, J., Gupta, S., Tada, R., Sinha, R., 2011. Improved provenance tracing of asian dust sources using rare earth elements and selected trace elements for palaeomonsoon studies on the eastern tibetan plateau. Geochim. Cosmochim. Acta 75, 6374–6399.

Ferrat, M., Weiss, D.J., Dong, S., Large, D.J., Spiro, B., Sun, Y., Gallagher, K., 2012. Lead atmospheric deposition rates and isotopic trends in asian dust during the last 9.5 kyr recorded in an ombrotrophic peat bog on the eastern Qinghai-tibetan plateau. Geochim. Cosmochim. Acta 82, 4–22.

Ferrat, M., Weiss, D.J., Spiro, B., Large, D., 2012. The inorganic geochemistry of a peat deposit on the eastern Qinghai-tibetan plateau and insights into changing atmospheric circulation in Central Asia during the holocene. Geochim. Cosmochim. Acta 91, 7–31.

Fiałkiewicz-Kozieł, B., Kołaczek, P., Piotrowska, N., Michczyński, A., Łokas, E., Wachniew, P., Woszczyk, M., Sensuła, B., 2014. High-resolution age-depth model of a peat bog in Poland as an important basis for paleoenvironmental studies. Radiocarbon 56, 109–125.

Fiałkiewicz-Kozieł, B., Smieja-Krol, B., Frontasyeva, M., Slowinski, M., Marcisz, K., Lapshina, E., Gilbert, D., Buttler, A., Jassey, V.E., Kaliszan, K., Laggoun-Defarge, F., Kolaczek, P., Lamentowicz, M., 2016. Anthropogenic- and natural sources of dust in peatland during the anthropocene. Sci. Rep. 6, 38731.

Fiałkiewicz-Kozieł, B., De Vleeschouwer, F., Mattielli, N., Fagel, N., Palowski, B., Pazdur, A., Smieja-Król, B., 2018. Record of anthropocene pollution sources of lead in disturbed peatlands from southern Poland. Atmos. Environ. 179, 61–68.

Fiałkiewicz-Kozieł, B., Łokas, E., Gałka, M., Kołaczek, P., De Vleeschouwer, F., Le Roux, G., Smieja-Król, B., 2020. Influence of transboundary transport of trace elements on mountain peat geochemistry (Sudetes, Central Europe). Quat. Sci. Rev. 230, 106162.

Franzén, L.G., 2006. Mineral matter, major elements, and trace elements in raised bog peat: a case study from southern Sweden, Ireland and Tierra del Fuego, south Argentina. Dev. Earth Surf. Proc. 9, 241–270.

Gallon, C., Ranville, M.A., Conaway, C.H., Landing, W.M., Buck, C.S., Morton, P.L., Flegal, A.R., 2011. Asian industrial Lead inputs to the North Pacific evidenced by Lead concentrations and isotopic compositions in surface waters and aerosols. Environ. Sci. Technol. 45, 9874–9882.

Geagea, M.L., Stille, P., Gauthier-Lafaye, F., Millet Perrone, Th., 2007. REE characteristics and pb, sr and nd isotopic compositions of steel plant emissions. Sci. Total Environ. 373, 404–419.

Geagea, M.L., Stille, P., Gauthier-Lafaye, F., Millet, M., 2008. Tracing of industrial aerosol sources in an urban environment using pb, sr, and nd isotopes. Environ. Sci. Technol. 42, 692–698.

Global Power Plants Database, 2018. https://datasets.wri.org/dataset/globalpowerplantdatabase.

Grousset, F.E., Biscaye, P.E., 2005. Tracing dust sources and transport patterns using Sr, Nd and Pb isotopes. Chem. Geol. 222 (3–4), 149–167.

Grousset, F.E., Ginoux, P., Bory, A., Biscaye, P.E., 2003. Case study of a Chinese dust plume reaching the French Alps. Geophys. Res. Lett. 30, 1277.

Herzschuh, U., Cao, X., Laepple, T., Dallmeyer, A., Telford, R.J., Ni, J., Chen, F., Kong, Z., Liu, G., Liu, K.B., Liu, X., Stebich, M., Tang, L., Tian, F., Wang, Y., Wischnewski, J., Xu, Q., Yan, S., Yang, Z., Yu, G., Zhang, Y., Zhao, Y., Zheng, Z., 2019. Position and orientation of the westerly jet determined holocene rainfall patterns in China. Nat. Commun. 10, 2376.

IEE-PES, 2008. https://www.ieee-pes.org/images/files/pdf/Chinas_Power_Industry_Milestones_IEEE_PES-20081010.pdf.

Jeong, G.Y., Kim, J.Y., Seo, J., Kim, G.M., Jin, H.C., Chun, Y., 2014. Long-range transport of giant particles in asian dust identified by physical, mineralogical, and meteorological analysis. Atmos. Chem. Phys. 14, 505–521.

Kamenov, G.D., Brenner, M., Tucker, J.L., 2009. Anthropogenic versus natural control on trace element and Sr–Nd–Pb isotope stratigraphy in peat sediments of Southeast Florida (USA), 1500 AD to present. Geochim. Cosmochim. Acta 73, 3549–3567.

Krachler, M., Mohl, C., Emons, H., Shotyk, W., 2003. Two thousand years of atmospheric rare earth element (REE) deposition as revealed by an ombrotrophic peat bog profile, Jura Mountains, Switzerland. J. Environ. Monit. 5 (1), 111–121.

Kurokawa, J., Ohara, T., Morikawa, T., Hanayama, S., Janssens-Maenhout, G., Fukui, T., Kawashima, K., Akimoto, H., 2013. Emissions of air pollutants and greenhouse gases over asian regions during 2000–2008: regional emission inventory in ASia (REAS) version 2. Atmos. Chem. Phys. 13, 11019–11058.
Kylander, M.E., Weiss, D.J., Peiteado, Varela E., Taboada Rodriguez, T., Martínez, Cortizas A., 2006. Archiving natural and anthropogenic lead deposition in peatlands. Dev. Earth Surf. Process. 9 (C), 479–497.
Kylander, M.E., Muller, J., Wüst, R.A., Gallagher, K., Garcia-Sanchez, R., Coles, B.J., Weiss, D.J., 2007. Rare earth element and pb isotope variations in a 52 kyr peat core from Lynch's crater (NE Queensland, Australia): proxy development and application to paleoclimate in the southern hemisphere. Geochim. Cosmochim. Acta 71, 942–960.
Le Roux, G., Shotyk, W., 2006. Weathering of inorganic matter in bogs. Earth Surf. Process. Landf. 9, 197–216.
Le Roux, G., Fagel, N., de Vleeschouwer, F., Krachler, M., Debaille, V., Still, P., Mattielli, N., van der Knaap, O., van Leeuwen, J.F.N., Shotyk, W., 2012. Volcano- and climate-driven changes in atmospheric dust sources and fluxes since the late glacial in Central Europe. Geology 40, 335–338.
Lee, J.J., Kim, C.H., 2012. Roles of surface wind, NDVI and snow cover in the recent changes in asian dust storm occurrence frequency. Atmos. Environ. 59, 366–375.
Lee, E.H., Sohn, B.J., 2009. Examining the impact of wind and surface vegetation on the asian dust occurrence over three classified source regions. J. Geophys. Res. 114, D06205.
Lempart, M., Derkowski, A., Luberda-Durnaś, K., Skiba, M., Błachowski, A., 2018. Dehydrogenation and dehydroxylation as drivers of the thermal decomposition of fe-chlorites. Am. Mineral. 103, 1837–1850.
Li, G., Chen, J., Yang, J., Conway, T.M., 2009. Natural and anthropogenic sources of east asian dust. Geology 37 (8), 727–730.
Liang, E.Y., Shao, X.M., Kong, Z.C., Lin, J.X., 2003. The extreme drought in the 1920s and its effect on tree growth deduced from tree ring analysis: a case study in North China. Ann. For. Sci. 60, 145–152.
Liang, E., Liu, X., Yuan, Y., Qin, M., Fang, X., Huang, L., Zhu, H., Wang, L., Shao, X., 2006. The 1920s drought recorded by tree rings and historical documents in the semi-arid and arid areas of northern China. Clim. Chang. 79, 403–432.
Liu, C.Q., Masuda, A., Okada, A., Yabuki, S., Fan, Z.L., 1994. Isotope geochemistry of Quaternary deposits from the arid lands in northern China. Earth Planet. Sci. Lett. 127, 25–38.
Liu, M., Westphal, D.L., Wang, S., Shimizu, A., Sugimoto, N., Zhou, J., Chen, Y., 2003. A high-resolution numerical study of the asian dust storms of april 2001. J. Geophys. Res. 108 (D23), 8653.
McKendry, I.G., Strawbridge, K.B., O'Neill, N.T., Macdonald, A.M., Liu, P.S., Leaitch, W.R., Anlauf, K.G., Jaegle, L., Fairlie, T.D., Westphal, D.L., 2007. Trans-Pacific transport of Saharan dust to western North America: a case study. J. Geophys. Res. 112, D01103.
Milecka, K., Kowalewski, G., Fiałkiewicz-Kozieł, B., Gałka, M., Lamentowicz, M., Chojnicki, B.H., Goslar, T., Barabach, J., 2017. Hydrological changes in the rzecin peatland (Central Europe) induced by anthropogenic factors: implications for carbon sequestration. The Holocene 27, 651–664.
Miyazaki, T., Kimura, J.I., Katakuse, M., 2016. Geochemical records from loess deposits in Japan over the last 210 kyr: lithogenic source changes and paleoclimatic indications. Geochem. Geophys. Geosyst. 17, 2745–2761.
Mukai, H., Furuta, N., Fujii, T., Ambe, Y., Sakamoto, K., Hashimoto, Y., 1993. Characterization of sources of lead in the urban air of Asia using ratios of stable lead isotopes. Environ. Sci. Technol. 27, 1347–1356.
Mukai, H., Tanaka, A., Fujii, T., Nakao, M., 1994. Lead isotope ratios of airborne particulate matter as tracers of long-range transport of air pollutants around Japan. J. Geophys. Res. 99, 3717–3726.
Mukai, H., Tanaka, A., Fujii, T., Zeng, Y., Hong, Y., 2001. Regional characteristic of sulfur and lead at several chinese urban sites. Environ. Sci. Technol. 35, 1064–1071.
Nakano, T., Yokoo, Y., Nishikawa, M., Koyanagi, H., 2004. Regional Sr–Nd isotopic ratios of soil minerals in northern China as asian dust fingerprints. Atmos. Environ. 38, 3061–3067.
Nakano, T., Nishikawa, M., Mori, I., Shin, K., Hosonoa, T., Yokoo, Y., 2005. Source and evolution of the "perfect asian dust storm" in early april 2001: implications of the Sr–Nd isotope ratios. Atmos. Environ. 39, 5568–5575.
Nikitina, E., Kotov, V., 1999. Solving transboundary air pollution conflict: a new framework for countries in transition. In: Lonergan, S.C. (Ed.), Environmental Change, Adaptation, and Security. Proceedings of the NATO Advanced Research Workshop on Environmental Change, Adaptation, and Security Budapest, Hungary, pp. 231–245 Ph.D. thesis.
Novak, M., Emmanuel, S., Vile, M.A., Erel, Y., Véron, A., Paces, T., Wieder, R.K., Vanecek, M., Stepanova, M., Brizova, E., Hovorka, J., 2003. Origin of lead in eight central european peat bogs determined from isotope ratios, strengths, and operation times of regional pollution sources. Environ. Sci. Technol. 37, 437–445.
Peng, Z., Zartman, R.E., Futa, K., Chen, D., 1986. Pb-, sr-and nd-isotopic systematics and chemical characteristics of cenozoic basalts, eastern China. Chem. Geol. 59, 3–33.
Pin, C., Briot, D., Bassin, C., Poitrasson, F., 1994. Concomitant separation of strontium and samarium-neodymium for isotopic analysis in silicate samples, based on specific extraction chromatography. Anal. Chim. Acta 298, 209–217.
Pratte, S., Mucci, A., Garneau, M., 2013. Historical records of atmospheric metal deposition along the St. Lawrence Valley (eastern Canada) based on peat bog cores. Atmos. Environ. 79, 831–840.
Pratte, S., De Vleeschouwer, F., Garneau, M., 2017. Geochemical characterization (REE nd and pb isotopes) of atmospheric mineral dust deposited in two maritime peat bogs from the st Lawrence north shore (eastern Canada). J. Quat. Sci. 32 (5), 617–627.
Pratte, S., Bao, K., Shen, J., Mackenzie, L., Klamt, A.-M., Wang, G., Xing, W., 2018. Recent atmospheric metal deposition in peatlands of Northeast China: a review. Sci. Total Environ. 626, 1284–1294.
Pratte, S., Bao, K., Sapkota, A., Zhang, W., Shen, J., Le Roux, G., De Vleeschouwer, F., 2020. 14 kyr of atmospheric mineral dust deposition in north-eastern China: a record of palaeoclimatic and palaeoenvironmental changes in the Chinese dust source regions. Holocene 30 (4), 492–506.
Purvis, O.W., Chimonides, P.J., Jones, G.C., Mikhailova, I.N., Spiro, B., Weiss, D.J., Williamson, B.J., 2004. Lichen biomonitoring near Karabash smelter town, Ural Mountains, Russia, one of the most polluted areas in the world. Proc. R. Soc. B Biol. Sci. 271 (1536), 221–226.
Qian, W., Quan, L., Shi, S., 2002. Variations of the dust storm in China and its climatic control. J. Clim. 15, 1216–1229.
Sapkota, A., 2006. Mineralogical, Chemical, and Isotopic (Sr, Pb) Composition of Atmospheric Mineral Dusts in an Ombrotrophic Peat Bog, Southern South America. University of Heidelberg, p. 182 PhD dissertation.
Sassen, K., 2002. Indirect climate forcing over the western US from asian dust storms. Geophys. Res. Lett. 29, 1465.
Schettler, G., Liu, Q., Mingram, J., Stebich, M., Dulski, P., 2006. East-asian monsoon variability between 15 000 and 2000 cal. yr BP recorded in varved sediments of Lake sihailongwan (north-Eastern China, long gang volcanic field). The Holocene 16, 1043–1057.
Schleicher, N.J., Dong, S., Packman, H., Little, S.H., Ochoa, Gonzalez R., Najorka, J., Sun, Y., Weiss, D.J., 2020. A global assessment of copper, zinc, and lead isotopes in mineral dust sources and aerosols. Front. Earth Sci. 8, 167.
Shotyk, W., 1988. Review of the inorganic geochemistry of peats and peatland waters. Earth Sci. Rev. 25 (2), 95–176.
Shotyk, W., Cheburkin, A.K., Appleby, P.G., Fankhauser, A., Kramers, J.D., 1997. Lead in three peat bog profiles, Jura Mountains, Switzerland: enrichment factors, isotopic composition, and chronology of atmospheric deposition. Water Air Soil Pollut. 100 (3-4), 297–310.
Shotyk, W., Cheburkin, A.K., Appleby, P.G., Fankhauser, A., Kramers, J.D., 1998. Lead in three peat bog profiles, Jura Mountains, Switzerland: enrichment factors, isotopic composition, and chronology of atmospheric deposition. Water Air Soil Pollut. 100 (3–4), 297–310.
Shotyk, W., Weiss, D., Appleby, P.G., Cheburkin, A.K., Frei, R., Gloor, M., Kramers, J.D., Reese, S., Van Der Knaap, W.Q., 1998. History of atmospheric lead deposition since 12,370 14C yr BP recorded in a peat bog profile, Jura Mountains, Switzerland. Science 281, 1635–1640.
Shotyk, W., Krachler, M., Martinez-Cortizas, A., Cheburkin, A.K., Emons, H., 2002. A peat bog record of natural, pre-anthropogenic enrichments of trace elements in atmospheric aerosols since 12 370 ^{14}C yr BP, and their variation with Holocene climate change. Earth Planet. Sci. Lett. 199 (1-2), 21–37.
Shotyk, W., Goodsite, M.E., Roos-Barraclough, F., Lohse, C., Hansen, T.S., 2003. Anthropogenic contributions to atmospheric hg, pb and as accumulation recorded by peat cores from southern Greenland and Denmark dated using the 14C "bomb pulse curve". Geochim. Cosmochim. Acta 67 (21), 3991–4011.
Shotyk, W., Rausch, N., Outridge, P.M., Krachler, M., 2016. Isotopic evolution of atmospheric Pb from metallurgical processing in Flin Flon, Manitoba: retrospective analysis using peat cores from bogs. Environ. Pollut. 218, 338–348.
Sjöström, J.K., Bindler, R., Granberg, T., Kylander, M.E., 2019. Procedure for organic matter removal from peat samples for XRD mineral analysis. Wetlands 39, 473–481.
Smieja-Król, B., Fiałkiewicz-Kozieł, B., 2014. Quantitative determination of minerals and anthropogenic particles in some polish peat occurrences using a novel SEM point - counting method. Environ. Monit. Assess. 186, 2573–2587.
Sun, J.M., Zhu, X., 2010. Temporal variations in pb isotopes and trace element concentrations within chinese eolian deposits during the past 8 ma: implications for provenance change. Earth Planet. Sci. Lett. 290 (3), 438–447.
Sun, J.M., Zhang, M.Y., Liu, T.S., 2001. Spatial and temporal characteristics of dust storms in China and its surrounding regions, 1960–1999: relations to source area and climate. J. Geophys. Res. Atmos. 106, 10325–10333.
Sun, J., Zhang, M., Liu, T., 2002. Spatial and temporal characteristics of dust storms in China and its surrounding regions, 1960–1999: relations to source area and climate. J. Geophys. Res. 106, 18325–18333.
Taylor, S.R., McLennan, S.M., 1985. Continental Crust: Its Composition and Evolution. An Examination of the Geochemical Record Preserved in Sedimentary Rocks. Blackwell Scientific Publications.
Van Der, A.R.J., Mijling, B., Ding, J., Elissavet, Koukouli M., Liu, F., Li, Q., Mao, H., Theys, N., 2017. Cleaning up the air: effectiveness of air quality policy for SO2 and NOx emissions in China. Atmos. Chem. Phys. 17, 1775–1789.
Vanneste, H., De Vleeschouwer, F., Bertrand, S., Martínez-Cortizas, A., Vanderstraeten, A., Mattielli, N., Coronato, A., Piotrowska, N., Jeandel, C., Roux, G.L., 2016. Elevated dust deposition in Tierra del Fuego (Chile) resulting from neoglacial Darwin cordillera glacier fluctuations. J. Quat. Sci. 31 (7), 713–722.
Wan, D., Yang, H., Jin, Z., Xue, B., Song, L., Mao, X., Yang, J., 2020. Spatiotemporal trends of atmospheric pb over the last century across inland China. Sci. Total Environ. 729, 138399.
Wang, S.W., Zhu, J.H., Cai, J.N., 2004. Interdecadal variability of temperature and precipitation in China since 1880. Adv. Atmos. Sci. 21, 307–313.
Wang, X., Zhang, C.X., Wang, H.T., Qian, G.Q., Luo, W.Y., Lu, J.F., 2011. The significance of Gobi desert surfaces for dust emissions in China: an experimental study. Environ. Earth Sci. 64, 1039–1050.
Wang, H., Jia, X., Li, K., Li, Y., 2015. Horizontal wind erosion flux and potential dust emission in arid and semiarid regions of China: a major source area for East Asia dust storms. Catena 133, 373–384.

Zdanowicz, C., Hall, G., Vaive, J., Amelin, Y., Percival, J., Girard, I., Biscaye, P., Bory, A., 2006. Asian dust fall in the St. Elias Mountains, Yukon, Canada. Geochim. Cosmochim. Acta 70, 3493–3507.

Zhang, X.Y., Arimoto, R., An, Z.S., 1997. Dust emission from Chinese desert sources linked to variations in atmospheric circulation. J. Geophys. Res. 102, 28,041–28,047.

Zhang, Q.G., Kang, S.C., Kaspari, S., Li, C.L., Qin, D.H., Mayewski, P.A., Hou, S.G., 2009. Rare earth elements in an ice core from mt. Everest: seasonal variations and potential sources. Atmos. Res. 94, 300–312.

Zhang, S., Xu, H., Lan, J., Goldsmith, Y., Torfstein, A., Zhang, G., Zhang, J., Song, Y., Zhou, K., Tan, L., Xu, S., Xu, X., Enzel, Y., 2021. Dust storms in northern China during the last 500 years. Sci. China Earth Sci. 64, 813–824.